Z. Kristallogr. Proc. **1** (2011) 15-20 / **DOI** 10.1524/zkpr.2011.0002

Differential Pair Distribution Function applied to $Ce_{1-x}Gd_xO_{2-x/2}$ system

M. Allieta[1], M. Brunelli[2,*], M. Coduri[1], M. Scavini[1], C. Ferrero[3]

[1] Dipartimento di Chimica Fisica ed Elettrochimica dell'Università di Milano, 20133 Milano, Italy
[2] Institut Laue Langevin, 6 av. J. Horowitz, BP 156, 38042 Grenoble Cedex 9, France
[3] European Synchrotron Radiation Facility, 6 av. J. Horowitz, BP 220, 38043 Grenoble Cedex 9, France
[*] Contact author; e-mail: brunelli@ill.fr

Keywords: Pair Distribution Function, anomalous dispersion; doped ceria

Abstract. The Pair Distribution Function technique based upon X-ray diffraction data is a powerful tool to unveil disorder on the nanometric scale, which is however element insensitive. To overcome this problem, Differential Pair Distribution Functions (DPDF) can be obtained by exploiting the anomalous dispersion of X-rays near the absorption edge of a certain element. In this paper the DPDF method is briefly reviewed and applied to the case of gadolinium doped ceria electrolytes. XRPD data have been collected at the Ce-*K* edge on the ID31 beamline of the European Synchrotron Radiation Facility (ESRF). The validity of this approach to extract chemical specific information is also briefly discussed.

Introduction

$Ce_{1-x}Gd_xO_{2-x/2}$ (CGO) compounds have been intensively studied in the last years as conducting electrolytes for electrochemical cells [1]. The ionic conductivity in CGO is due to oxygen diffusion via the vacancy mechanism. Actually, half oxygen vacancy is introduced into the structure when a Ce^{4+} ion is substituted by a Gd^{3+} one. At increasing Gd^{3+} concentration x, the conductivity $\sigma_i(x)$ reaches a maximum (at fixed T) and then decreases for higher x values [2]. This behaviour has been attributed to the formation of defect clusters.
Accordingly, EXAFS measurements have detected the presence of Gd^{3+}-V_O-Gd^{3+} defect clusters in CGO materials [3]. However, the EXAFS technique can be successfully employed to explore *only* the local structure of Ce^{4+} and Gd^{3+} ions, and cannot provide further information in case of more extended defects (e.g. on the nanometric scale).
In contrast, the Pair Distribution Function (PDF) $G(r)$, i.e. the real space analysis of diffraction data, is a unique tool to determine the local and medium range deviations with respect to an ideally periodic structure within the same X-ray powder diffraction (XRPD) experiment.
However, unlike EXAFS, this technique is not element sensitive, therefore it can be difficult to discriminate the contributions of Ce^{4+} and Gd^{3+} ions since their ionic radii are similar.

This problem can be overcome by applying the anomalous X-ray diffraction (AXD) technique [4] to a total scattering method in order to obtain the so-called Differential Pair Distribution Function (DPDF) [5].

As a part of a wider study on the local and medium range structure in CGO compounds, we discuss the applicability of the DPDF technique to these systems. For this purpose the DPDF principle is reviewed and its basic equations are reported. Finally, the DPDF application to XRPD data collected close to the Ce *K*-edge is shown. The validity of this approach to obtain chemical specific information is briefly discussed.

Experimental

A micro-crystalline CGO sample with Gd concentration x =0.25 was prepared with the *Pechini* sol-gel method and fired at 900°C for 72 hours. XRPD patterns were collected at the ID31 beamline of the ESRF in the diffraction range $0<2\theta<80°$ covering a range of the wavevector Q ($=4\pi \sin\theta/\lambda$) up to Q_{max}~30 Å^{-1}. We collected experimental data (plus empty capillary and air background) from a $Ce_{0.75}Gd_{0.25}O_{1.875}$ sample at incident X-ray wavelengths λ_1=0.30975(1) Å and λ_2=0.30760(1) Å, respectively, near the Ce *K*-absorption edge. Additional data at λ_1 were collected also on CeO_2 (Aldrich ≥99.0%) and Gd_2O_3 (Aldrich 99.9%). In order to attain XRPD data quality for experimental $G(r)$, all patterns were obtained summing several scans (~7 hours total measuring time) performed at fixed temperature (T=90K). Data were corrected using the PDFGetX2 software [6]. In order to avoid an excessive noise-to-signal ratio at high Q range in the DPDF we have considered only data up to Q_{max}=24 Å^{-1} for all the samples. An X-ray fluorescence measurement was carried out on CeO_2 in the $39.93<E<40.62$ keV energy range across the Ce *K*-edge.

Differential Pair Distribution Function at the Ce *K*-edge: Method and results

The total PDF, $G(r)$, is the atomic number density-density correlation function which describes atomic arrangements in powders or isotropically scattering amorphous materials [5]. The $G(r)$ function is obtained through the total structure factor S(Q) via the sine Fourier Transform (FT) [5]:

$$G(r) = 4\pi r[\rho(r) - \rho_0] = \frac{2}{\pi}\int_{Q=0}^{Q_{max}} Q[S(Q) - 1]\sin(Qr)\mathrm{d}Q \qquad (1)$$

Here, $\rho(r)$ and ρ_0 are the local and average atomic number densities and r is the interatomic distance. The upper integration limit Q_{max} is the reciprocal space cut-off.

For a single diffraction experiment on a sample composed of n chemical species, the total structure factor can be expressed as a weighted average of $n(n+1)/2$ partial structure factors [5], i.e.:

$$S(Q) - 1 = \sum_{i,j}^{n} \frac{c_i c_j f_i(Q,\lambda) f_j(Q,\lambda)}{< f(Q,\lambda) >^2}[S_{ij}(Q) - 1] \qquad (2)$$

where c_i is the atomic fraction of the j component and $f_i(Q,\lambda)$ is the atomic scattering factor of the i component. The double sum runs over all atoms of the sample's stoichiometric unit

and the brackets < > mean the average over the compound unit. $S_{ij}(Q)$ is the partial structure factor of the (i,j) atoms pair.
The total structure factor is calculated from the experimental coherent X-ray scattering intensity $I^{coh}(Q,\lambda)$ by:

$$S(Q) - 1 = \frac{I^{\text{coh.}}(Q,\lambda) - < f^2(Q,\lambda) >}{< f(Q,\lambda) >^2} \tag{3}$$

Combining equations (2) and (3) yields:

$$I^{\text{coh.}}(Q,\lambda) - < f^2(Q,\lambda) >= \sum_{i,j}^{n} c_i c_j f_i(Q,\lambda) f_j(Q,\lambda)[S_{ij}(Q) - 1] \tag{4}$$

From equation (4), it can be seen that all $S_{ij}(Q)$ can be determined from $n(n-1)/2$ independent intensity measurements according to which the atomic fractions in this equation are varied. A way to produce a significant change in the factors $f_i(Q,\lambda)$ is to exploit the anomalous dispersion effect of the X-rays near the absorption edge of an element [7]. Complete experimental and theoretical details of the anomalous X-ray scattering technique are reported elsewhere [4] and in the following we briefly present the application of this technique to obtain chemical specific $G(r)$ functions.
The atomic scattering factor of a specific atom is given by:

$$f(Q,E) = f_0(Q) + f'(E) + if''(E) \tag{5}$$

where the $f_0(Q)$ is the scattering factor and $f'(E)$ and $f''(E)$ are the real and imaginary part of the anomalous dispersion term, respectively.
The trends of $f'(E)$ and $f''(E)$ versus E in the close vicinity of an absorption edge (Ce K-edge) are shown in Figure 1 (solid lines). The $f''(E)$ term is directly related to the photoelectric absorption and is almost flat below the edge and rises dramatically at the edge. $f'(E)$ exhibits a sharp negative peak with a full width at half maximum of ~100eV. According to equation (4), if two diffraction intensity measurements are performed at slightly different wavelengths λ_1, λ_2 near the absorption edge of a particular element A, a large change of the real part of $f_A(Q,\lambda)$ and consequently of the coherent Intensity $I^{coh}(Q,\lambda)$ occurs. The differential structure factor ($DSF(Q)$) is defined as [8]:

$$DSF(Q) \equiv \frac{[I^{\text{coh.}}(Q,\lambda_1) - < f^2(Q,\lambda_1) >] - [I^{\text{coh.}}(Q,\lambda_2) - < f^2(Q,\lambda_2) >]}{c_A[f'(\lambda_1) - f'(\lambda_2)]\mathrm{W}(Q,\lambda_1,\lambda_2)} = \sum_{j}^{n} \frac{\mathrm{W}_{Aj}(Q,\lambda_1,\lambda_2)}{\mathrm{W}(Q,\lambda_1,\lambda_2)}[S(Q)_{Aj} - 1] \tag{6}$$

where the total $\mathrm{W}(Q,\lambda_1,\lambda_2)$ and partial $\mathrm{W}_{Aj}(Q,\lambda_1,\lambda_2)$ weighting factors are defined as follows:

$$\mathrm{W}(Q,\lambda_1,\lambda_2) = \sum_{k}^{n} c_k \Re[f_k(Q,\lambda_1) + f_k(Q,\lambda_2)] \tag{7}$$

$$\mathrm{W}_{Aj}(Q,\lambda_1,\lambda_2) = c_j \Re[f_j(Q,\lambda_1) + f_j(Q,\lambda_2)] \tag{8}$$

where $\Re$ stands for real part. According to equation (1), the DPDF is calculated from the FT of the $DSF(Q)$ function. The DPDF will then contain only contributions of atomic pairs involving the anomalously scattering atom.

The procedure shown above was applied to the case of a $Ce_{0.75}Gd_{0.25}O_{1.875}$ sample at the Ce *K*-edge.

In order to obtain experimental $f'(E)$ and $f''(E)$ values, the fluorescence spectrum of CeO_2 was measured and then converted to $f''(E)$ data and $f'(E)$ using the Kramers-Kronig (KK) relation [7](see Figure 1). Referring to pre-edge region ($E_1<E<E_2$ in Figure 1), the experimental values can be affected by instrumental aberration (e.g. large background) and the core hole lifetime broadening problem characterizing the *K*-edge of element with large atomic number Z. As these features cause the $f''(E)$ values to be unreliable near the Ce *K*-edge, in the present investigation the theoretical values for Ce were used [9]. However, it should be noted that for finely tuning the wavelengths involved in the present experiment, the determination of the fluorescence spectra is rather important to detect any monochromator offset.

To evaluate consistently $I^{coh.}(Q,\lambda)$ at each wavelength, the raw $I(Q,\lambda)$ were corrected for background scattering, attenuation in the sample, multiple and Compton scattering. In particular, at high Q the Compton scattering was removed by calculating the Compton profile with an analytical formula [5]. In the middle-low Q region the Compton scattering correction was applied by multiplying the calculated Compton profile with a monochromator cut-off function [5]. The corrected $I(Q, \lambda)$ were normalized using the $20Å^{-1}<Q<24Å^{-1}$ range of the experimental curves [5]. In Figure 2 (left) the normalized coherent intensities after correction $I^{coh.}(Q,\lambda_1)$ and $I^{coh.}(Q,\lambda_2)$ are reported. In the related inset the Q-behaviours of the average mean-square scattering factors required to apply equation (5) are also displayed. The non dispersive part of $f(Q,\lambda)$ was calculated for each ion using the analytical formula suggested in [10]. By taking the difference between the two curves, as shown in Figure 2 (right), the Ce related $DSF(Q)$ was calculated according to equation (5).

In order to test the validity of this method for the CGO system, we performed PDF quality measurements as described in section 2. In Figure 3 (left), the total PDFs obtained at λ_1 on pure CeO_2 and Gd_2O_3, respectively, are shown. The vertical dashed line centred on r~4.1Å indicates a $G(r)$ peak related to Gd-Gd distances pertaining only to the C-type structure of pure Gd_2O_3. Since this peak is absent in the CeO_2 fluoritic structure, it can be considered a clear fingerprint of the Gd contribution to the $G(r)$ function. Figure 3 (right) shows the PDF referring to pure CeO_2 together with the DPDF and the total PDF of the $Ce_{0.75}Gd_{0.25}O_{1.875}$ sample at λ_1. The peak at r~4.1Å is present in the total PDF pertinent to the $Ce_{0.75}Gd_{0.25}O_{1.875}$ sample while it is completely absent in the DPDF one.

Since the partial structure factor $[S_{GdGd}(Q)-1]$ is not involved in the $DSF(Q)$ (see equation (5)), the observation confirms the reliability of the differential approach in providing element sensitive information.

As a final comment, by comparing the DPDF and the total PDF for pure CeO_2 a fairly good agreement is obtained up to 6 Å. This suggests that Ce^{4+} ions retain their local environment as in CeO_2 and extended defect clusters (cationic compositional fluctuations) should occur in CGO materials. Further investigations are planned to fathom this experimental result, using both total and differential PDF techniques.

Conclusion

We have discussed the applicability of the DPDF approach to the CGO system. PDF quality measurements have been performed at two different wavelengths close to the Ce *K*-edge on a

$Ce_{0.75}Gd_{0.25}O_{1.875}$ sample at 90 K. The comparison of the total with the differential PDF of this sample reveals the disappearance of a peak at r~4.1Å in the latter. Since the partial structure factor [$S_{GdGd}(Q)$-1] is not involved in the $DSF(Q)$, this observation supports the idea that the differential approach can be successfully applied to this kind of samples.

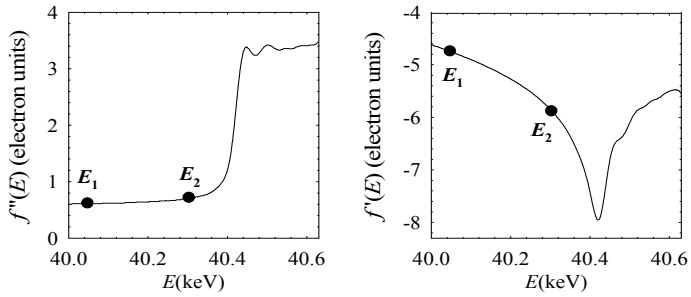

Figure 1. Energy dependence of the real f ′(E) and imaginary f″(E) part of the atomic X-ray scattering factor of CeO_2 near the Ce K-absorption edge. Solid lines are experimental data. The energies used in the anomalous scattering experiment are marked by dots.

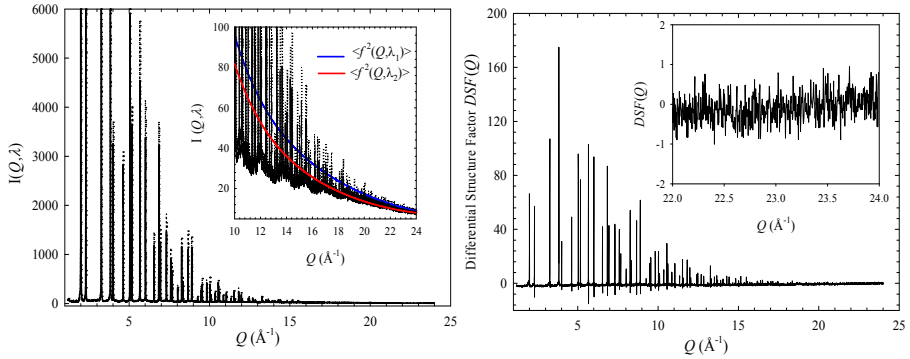

Figure 2. Left: Comparison between normalized and corrected coherent I(Q,λ) data, as collected at λ_1 (dotted line) and λ_2 (solid line). In the inset: Q-dependence of the average mean square atomic scattering factors. Right: reduced Ce differential structure factor for $Ce0_{.75}Gd_{0.25}O_{1.875}$. The inset shows the high Q-region. The asymptotic behaviour of the DSF(Q) testifies the correctness of the normalisation.

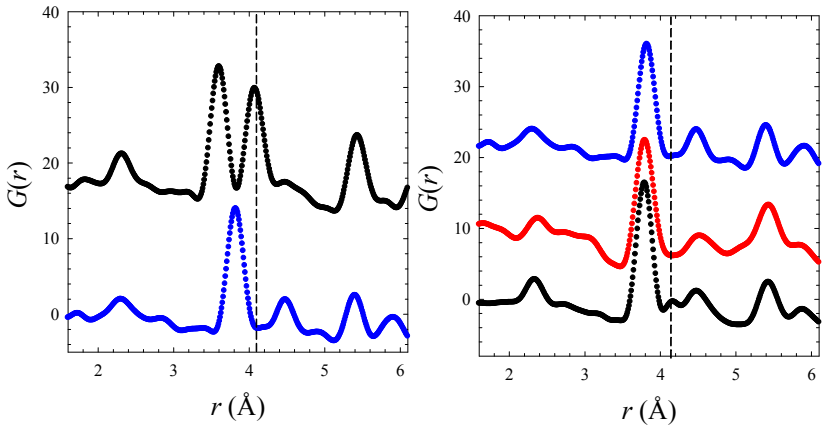

Figure 3. Left: total PDF for pure Gd_2O_3 (black dots) and CeO_2 (blue dots). The vertical dashed line shows the C-type Gd-Gd distance. Right: total (black dots) and differential (red dots) PDF for $Ce0.75Gd0.25O1.87$. The total PDF for pure CeO_2 is also shown (blue dots). The vertical line indicates again the same C-type Gd-Gd distance.

References

1. Goodenough, J., 2003, *Ann. Rev. Mater. Res.*, **33**, 91.
2. Zhang, T.S., Ma, J., Kong, L.B., Chan, S.H. & Kilner, J.A., 2004, *Solid State Ionics*, **170**, 209.
3. Deguchi, H., Yoshida, H., Inagaki, T. & Horiuchi, M., 2005, *Solid State Ionics*, **176**, 1817.
4. Waseda, Y., 1984, in *Novel Applications of Anomalous (Resonant) X-ray Scattering for Structural Characterization of Disordered Materials* (Berlin: Springer).
5. Egami, T. & Billinge, S.J.L., 2003, *Underneath the Bragg peaks: Structural Analysis of Complex Materials* (Pergamon Materials Series, V. 7).
6. Qiu, X., Thompson, J.W. & Billinge, S.J.L., 2004, *J. Appl. Crystallogr.*, **37**, 678.
7. Fischer, H.E. & Barnes, A.C., 2006, *Rep. Prog. Phys.*, **69**, 233.
8. Saito, M. & Waseda, Y., 2000, *J. Synchr. Rad.*, **7**, 152.
9. Sánchez del Río, M. & Dejus, R.J., 2004, *XOP 2.1: A new version of the X-ray optics software toolkit*,"Synchrotron Radiation Instrumentation: Eighth International Conference, edited by T. Warwick et al. (American Institute of Physics), pp 784-787.
10. Waasmaier, D. & Kirfel, A., 1995, *Acta Crystallogr. A*, **51**, 416.

Acknowledgements. The authors acknowledge the European Synchrotron Radiation Facility for provision of beam time; they also wish to thank Dr A.N. Fitch for assistance in using the ID31 beamline and Dr H.E. Fischer for useful discussions.